Persistent spectral hole burning in deuterated $CaF_2:Tm^{3+}$

N. M. Strickland and R. L. Cone
Department of Physics, Montana State University, Bozeman, Montana 59717-3840

R. M. Macfarlane
IBM Almaden Research Center, 650 Harry Road, San Jose, California 95120-6099

(Received 23 November 1998)

We report spectral hole burning in the deuteride (D^-) modified Tm^{3+} centers in CaF_2, where the hole burning mechanism is known to involve localized displacement of the D^- ions. Two main families of Tm^{3+}-D^- centers are present; the L*i* centers yield spectral holes that have been measured to be fully persistent for 48 hours at liquid-helium temperatures, while spectral holes of the M*i* centers have a hole-recovery time constant of approximately 20–30 s. Hole widths vary from 18–40 MHz (full width at half maximum) for the different centers. Burn-down curves are in agreement with a simple and general model that takes into account the finite homogeneous linewidth but makes no other assumptions about the nature of the hole burning mechanism. The area of the spectral holes is found to be conserved after the sample temperature has been cycled to up to 70 K, while the hole profile is broadened by this process. [S0163-1829(99)10721-5]

I. INTRODUCTION AND MOTIVATION

Persistent spectral hole burning is a powerful technique for high-resolution spectroscopy and also allows controlled modification of the absorption profile of an inhomogeneously broadened spectral line. Many possible applications have been described[1] exploiting the high-frequency resolution and programmable nature of persistent spectral hole burning, including frequency-domain[2,3] and time-domain[4–6] optical data storage, amplitude and temporal pulse shaping,[7–9] holographic image storage,[6,10] frequency-multiplexed optical filtering,[11] cw laser beam modulation,[12] and optical computing.[13] In addition, we are currently exploring passive optical routing and frequency reference applications. For such applications, the principal hole burning parameters that characterize the device performance are the persistence, spectral width, and saturation depth of the hole. In addition, the transition energy is important in determining the availability and cost of an appropriate single-frequency laser source.

Almost all previously reported cases of persistent spectral hole burning in rare-earth doped crystals involve photoionization of the rare earth as the hole burning mechanism, limiting such observances to specific ions and hence specific wavelengths.[14–16] The hole burning mechanism that applies to rare-earth transitions in deuterated CaF_2 involves D^- ion displacement.[17,18] This mechanism is host specific, rather than dopant-ion specific, and it therefore provides greater wavelength versatility by allowing the relatively free choice of rare-earth dopant. Site-distortion mechanisms for hole burning are often found in rare-earth-doped glasses but are unusual for crystalline hosts. Other site-distortion mechanisms in crystals have been reported for $SrWO_4:U^{6+}$ and $BaWO_4:U^{6+}$ (Ref. 19) and $CeF_4:Cm^{4+}$.[20]

Here, we report a study of persistent spectral hole burning on the $^3H_6 \rightarrow {}^3H_4$ transition of deuteride compensated Tm^{3+} centers in CaF_2. This transition of Tm^{3+}-doped materials is of particular interest for applications since it typically lies near 800 nm, in a wavelength region conveniently accessible by cheap and compact GaAlAs diode lasers. For one D^- compensated center, hole depth was preserved for over 48 h with no observable changes. No other Tm^{3+}-doped crystal, to our knowledge, exhibits persistent spectral hole burning. Indeed other Tm^{3+} systems typically exhibit millisecond time scale hole lifetimes.[21]

A. D^--compensated rare-earth centers

Three main single Tm^{3+} ion centers are found in undeuterated $CaF_2:Tm^{3+}$.[22] The principal center is the C_{4v}-symmetry *A* center in which the Tm^{3+} ion is charge compensated by an F^- ion in the nearest-neighbor interstitial position in the (001) direction. The secondary *B* center with C_{3v} symmetry was initially proposed to have its charge compensating F^- ion in the next-nearest-neighbor position in the (111) direction, but more complex configurations have since been suggested to account for the observed dielectric relaxation and anomalous crystal-field splittings.[23,24] The *A* and *B* centers undergo millisecond time scale transient hole burning from population storage in the metastable $^3F_4$ level.[21] For the cubic center with remote charge compensation, electric-dipole transitions such as the $^3H_6 \rightarrow {}^3H_4$ transition studied in this report are forbidden by inversion-symmetry selection rules. However, the cubic center is known to be present in $CaF_2:Tm^{3+}$ as evidenced by the magnetic-dipole allowed $^3H_6 \rightarrow {}^3H_5$ transition.[22]

The introduction of negative deuteride (D^-) ions into rare-earth-doped CaF_2 crystals produces a series of new rare-earth centers that involve D^- ions substituting for interstitial or lattice F^- ions in the vicinity of the rare-earth ion. These centers give rise to a series of additional sharp absorption lines and can therefore be probed selectively using a tunable laser.[18,22,25] $CaF_2:Pr^{3+}:D^-$ and the closely related $SrF_2:Pr^{3+}:D^-$ are the most extensively explored of these systems, and site configuration models have been proposed[18] for the D^- compensated centers from the polarized laser se-

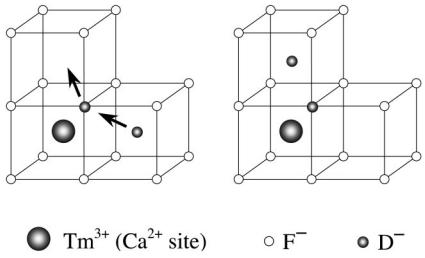

FIG. 1. Proposed site configuration of the L1 spectroscopic center, and the D^- ion displacement mechanism responsible for persistent spectral hole burning of this center; (a) the original configuration, and (b) the photoproduct configuration.

lective excitation spectroscopy and bleaching dynamics. In these models, the rare-earth ion is charge compensated by an interstitial D^- ion residing at the nearest-neighbor interstice, in the (100) direction. The C_{4v} symmetry of this configuration can then be reduced by the substitution of further D^- ions for the F^- ions of the lattice. The simplest of these low-symmetry centers, having one substitutional D^- ion in addition to the interstitial, is represented in Fig. 1. For heavier rare earths, such as Er^{3+} and Tm^{3+}, a second family of centers appears.[22,25] These are most likely based on the C_{3v} symmetry configuration of the *B* center.

For the Tm^{3+} centers reported here the first group of deuteride-compensated centers, derived from the *A* center, have been labeled L*i*$(i=0,1,2,3)$[22] where L0 is the C_{4v} symmetry center with only one D^- ion. The second group of deuteride-compensated centers, presumed to derive from the *B* center, are labeled M*i*.

B. Hole burning mechanism

The absorption transitions of the low-symmetry multiple-D^- compensated rare-earth centers can be bleached upon pumping with a tunable laser. Such bleaching using a broadband laser with linewidth similar to the absorption linewidth has been reported for several rare-earth ions in such sites.[18,22,25] The extension to spectral hole burning with a narrow-band laser has been reported for the Pr^{3+}-doped CaF_2 and SrF_2 systems.[17]

The bleaching behavior has been well characterized for the L*i* centers, and the mechanism involves local displacement of the D^- ions in the vicinity of the rare-earth ion.[18] From the reduced fluorescence lifetime of these centers, it is known that the principal relaxation pathway for the photoexcited rare-earth ion is to transfer its energy to multiple high-energy (700 cm^{-1}) local-mode vibrations of adjacent D^- ions. These excited D^- ions then have some chance of migrating into nearby interstices. The stepwise process illustrated in Fig. 1 illustrates the necessity of a substitutional D^- ion; the substitutional D^- ion moves into a vacant interstitial position and the interstitial D^- ion takes its place at the substitutional site. This proposed mechanism is supported by the absence of any bleaching behavior for the C_{4v} center involving just a single D^- ion for any of the rare earths studied to date, showing that a direct tunneling process from one interstitial site to another does not occur at low temperature.

In some cases, such as for the center illustrated in Fig. 1, the photoproduct center is equivalent to the original but has its dipole axis reoriented. This gives rise to the polarized reversible bleaching in the broadband pumping case. However, in the hole burning regime the reoriented photoproduct will experience different local strains from the original center. In general, its resonance frequency will be shifted randomly within the inhomogeneous absorption profile, and therefore a distinct antihole is not produced. The bleaching behavior for the M*i* centers has not been studied in any detail, but the involvement of D^- ion motion is clear.

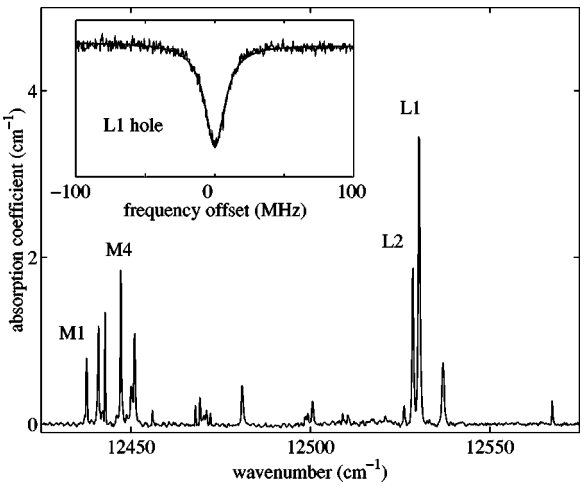

FIG. 2. Absorption spectrum of the $^3H_4$ multiplet of Tm^{3+} ions in deuterated CaF_2. Major absorption features that displayed spectral hole burning are labeled. Inset: a persistent spectral hole burned in the L1 center absorption line, and Lorentzian fit, giving a holewidth of 18 MHz.

II. EXPERIMENT

The $^3H_4$ absorption lines of Tm^{3+} in CaF_2:Tm^{3+}:D^- were excited and detected using a tunable Coherent 899-21 single-frequency Ti:sapphire laser, pumped by a Coherent Sabre argon-ion laser and intensity-stabilized by a Laser Power Controller from Cambridge Research & Instrumentation. The holes were probed by measuring the transmission of the laser using a Hamamatsu R928 photomultiplier tube, at laser intensities reduced by 1 to 2 orders of magnitude relative to the burn intensity. Sample temperatures could be controlled anywhere between 1.5 and 300 K in an Oxford Instruments Optistat-Bath cryostat and were determined using a Lake Shore Cryotronics carbon-glass resistance thermometer. Sample temperatures were typically between 1.5–2 K, unless otherwise stated.

A. Absorption spectrum, site identification

The CaF_2 crystal was grown using the Czochralski method, with 0.05% (molar) TmF_3 added in the melt. Deuteration was achieved by baking the sample for 48 h at 850 °C in 2/3 atmosphere of deuterium gas and in contact with aluminum metal. The absorption spectrum of the Tm^{3+} $^3H_4$ multiplet for the deuterated crystal is shown in Fig. 2. Due to transition selection rules and the broadening of upper levels, the absorption spectrum of the parent, undeuterated crystal has only one sharp absorption line for each of the C_{4v} and C_{3v} F^- centers in this frequency range,[22] and

TABLE I. Characteristic parameters of the $^3H_4$ absorption lines of each major Tm^{3+} center in the deuterated $CaF_2:Tm^{3+}$ sample studied.

Line center (cm^{-1})		Peak height (cm^{-1})	Linewidth (cm^{-1})	Line strength (cm^{-2})	Estimated concentration[a] $\times 10^{16}$ cm^{-3}
12438.8	(M1)	0.79	0.41	0.51	10
12442.1		1.18	0.38	0.70	20
12443.9		1.34	0.30	0.63	10
12448.3	(M4)	1.85	0.37	1.08	20
12452.2		1.09	0.46	0.79	20
12457.1		0.16	0.30	0.08	2
12469.1		0.22	0.27	0.09	2
12470.3		0.32	0.35	0.17	4
12472.2		0.17	0.46	0.12	3
12482.1		0.46	0.56	0.40	9
12501.7		0.27	0.53	0.23	5
12527.3		0.22	0.45	0.15	3
12529.7	(L2)	1.87	0.52	1.52	30
12531.4	(L1)	3.45	0.60	3.23	70
12538.1	C_{4v} (D^-)	0.73	0.70	0.81	20
12568.5	C_{4v} (F^-)	0.28	0.36	0.16	4
12599.1		0.17	0.38	0.10	2

[a]See text for assumptions made.

the remaining absorption lines in the spectrum of the deuterated crystal are due to D^- ion compensated centers.

The absorption transitions in Fig. 2 are clearly divisible into groups of transitions corresponding to the two types of centers. The higher energy group, near 12 530 cm^{-1}, is due to the L*i* centers, with only one line per center, and these lines exhibit the expected reversible polarized bleaching behavior under broadband pumping conditions. The second group of lines near 12 440 cm^{-1} corresponds to the M*i* centers, and these may have one or two lines per center, since the corresponding line of the *B* center is known to be a singlet-doublet transition.[21]

Four of the absorption lines, labeled in the absorption spectrum, give long-term or medium-term persistent spectral hole burning. The centers giving rise to these lines are labeled L1, L2, M1, and M4. Table I lists the peak absorption coefficient and linewidth of each of the absorption lines in the deuterated sample. In order to estimate the hole burning quantum efficiency (Sec. II C), we require the absolute concentration of each center, which in turn requires that we know the oscillator strength of the absorption transition. Previous methods for determining transition oscillator strengths have depended on measuring the radiative transition rate from the level lifetime;[26] however, in this case the population decay is almost entirely nonradiative through relaxation by D^- localized vibrations, making direct determination of radiative transition rates impossible.

A very crude estimate of the concentration of each center is obtained here by assuming the entire concentration of Tm^{3+} ions in the crystal to be 0.01% (molar), allowing for only partial integration of the TmF_3 into the CaF_2 crystal and for the presence of the spectroscopically inert cubic center, and by taking the oscillator strength of each transition to be the same. This last assumption is weak, particularly when comparing between the two families of centers, but it provides the only simple means of estimating individual center concentrations.

TABLE II. Characteristic spectral hole burning parameters of the four centers which were found to give long-term spectral hole burning.

Center	Hole FWHM (MHz)	Quantum efficiency ($\times 10^{-4}$)	Recovery time (s)
L1	18	8	$>10^{6}$ [a]
L2	30	20	$>10^{5}$ [a]
M1	20	300	23
M4	40	100	23

[a]Lower limit for persistence dependent on measurement duration (see Sec. II B).

B. Persistent spectral hole burning

Of the four absorption lines that exhibit hole burning, two are from L*i*-type centers and two from M*i*-type centers and as noted earlier these have qualitatively different persistence behaviors. The L*i*-center holes did not show any measurable change over 48 h, the longest period measured, while the M*i*-center holes have decay constants of less than a minute. A representative spectral hole burned in the L1 absorption peak is shown in the inset of Fig. 2. Typically, a laser intensity of 1 mW/cm^2 was used for burning, and this was reduced by one to two orders of magnitude for the scan cycle. In this regime, shallow holes took tens of seconds to burn, while burning during the scan cycle was minimized. A relatively large laser spot size of 2–3 mm was used to provide sufficient total power for efficient detection. Hole burning parameters for each center are listed in Table II.

The hole widths listed in Table II are much broader than those that have been measured in the transient regime in undeuterated $CaF_2:Tm^{3+}$ (Ref. 21) or those associated with this transition of the Tm^{3+} ion in other ionic crystals, but they are similar to those observed in $CaF_2:Pr^{3+}:D^-$.[17] Neither fluorescence lifetime nor nuclear spin-flip processes can account for the extra dephasing in these deuterated Tm^{3+} systems; the nonmagnetic Tm^{3+} states are relatively insensitive to local magnetic-field fluctuations arising from F^- or D^- nuclear spins. It is possible that spectral diffusion, due to D^- motion at one Tm^{3+} site affecting the resonance frequency at another Tm^{3+} site, is responsible for the width.

No decay of the hole amplitude or area was seen for the L1 center for up to 48 h after burning. The persistence of the L1 hole is represented in Fig. 3, where the peak hole intensity and the hole area are plotted as functions of time after burning. A series of open circles plotted for the period between 31 and 39 h shows a period where the sample temperature was inadvertently allowed to increase to 5.2 K, leading to broadening of the hole, which reduced the hole peak but conserved the hole area. When the sample was cooled back to its initial temperature of 1.7 K, the hole recovered its original depth and width. See Sec. II E for details of hole recovery after temperature cycling. Overall, no discernible

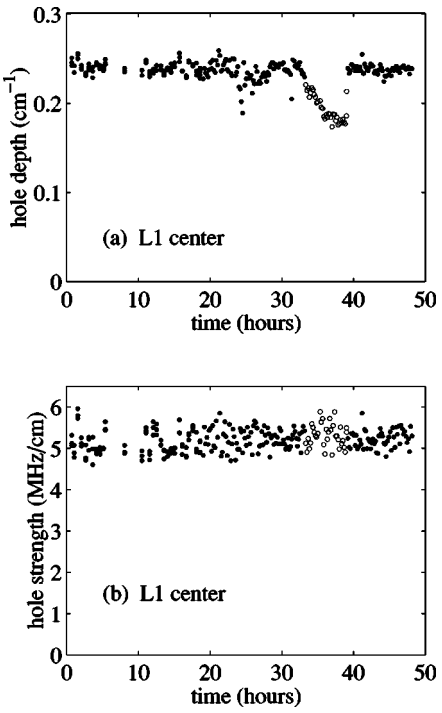

FIG. 3. Persistence of the L1-center spectral hole parameters; (a) the peak hole depth and (b) the hole area up to 48 h after burning. The open circles denote a period where the sample temperature was uncontrolled and increased up to 5.2 K. From this data and the temperature dependent studies, one may conclude that these holes persist at least for several weeks at liquid-helium temperatures.

degradation could be observed over 48 h. Attempts to impose an exponential decay curve on the data yield a lower bound on the decay time constant of the order of several weeks.

Hole degradation would be expected to manifest itself in two ways. First, simple hole decay, in which photo-transformed ions resume their original configurations, would be expected to reduce the peak intensity without greatly affecting the hole width, thus reducing the area. Second, spectral diffusion effects, where the hole broadens, would increase the width and reduce the peak intensity without changing the hole area. No mechanism for increasing the hole area at a fixed sample temperature is expected. Since any hole degradation effects would be expected to reduce the peak intensity of the hole, the smoother plot of the hole peak intensity in itself shows that the hole undergoes neither decay nor spectral diffusion, within the uncertainty of measurement, for at least 48 h.

The persistence of spectral holes in the L2 center was tested for 7 h, with a similar lack of degradation. In contrast, spectral holes burned in the M1 and M4 absorption lines decayed with time constants of 23 s with the sample in the dark at 1.7 K.

C. Model for hole burning curves

The quantum efficiency η has been defined as the probability of an ion being bleached from the absorption profile once it has absorbed a photon;[27] in this case this translates to the probability of an excited Tm^{3+} ion inducing site reorientation due to D^- ion motion. Thus

$$\eta = -\frac{dN}{dt} \Big/ \frac{(I_0 - I)}{h\nu L}, \tag{1}$$

where N is the concentration of the absorbing centers, I is the transmitted intensity, I_0 is the incident intensity, and L is the length of the sample. The denominator in this equation simply gives the number of photons absorbed per unit volume.

This equation does not explicitly take into account the finite spectral widths of the laser or of the homogeneous line. In the case of $CaF_2:Tm^{3+}:D^-$, the laser linewidth is much less than the narrowest measured hole width and it suffices to consider the homogeneous line profile only. Such a model has been considered previously,[28] and the principal features are outlined here.

We consider the concentration of absorbing ions per unit frequency as a function of their resonant frequency $N(\nu)$. Initially we can assume this to be a flat function as the inhomogeneous line profile is much larger than the hole widths. The homogeneous line shape for a single ion centered at ν' is represented by the normalized function $\kappa(\nu - \nu')$. This line shape is taken to be Lorentzian for this model. For the population of ions at a given frequency ν, the bleaching rate will be proportional to the incident laser intensity I_0, the hole burning quantum efficiency η, the absorption cross section σ, the population of these ions $N(\nu)$, and the overlap of the homogeneous line shape with the laser frequency $\kappa(\nu - \nu_0)$. Thus

$$\frac{dN(\nu)}{dt} = -\frac{\eta I_0 N(\nu)\sigma\kappa(\nu_0 - \nu)}{h\nu_0} \tag{2}$$

which yields the solution

$$N(\nu) = N_0(\nu)\exp\left\{-\frac{\eta I_0 \sigma\kappa(\nu_0 - \nu)}{h\nu_0}t\right\}. \tag{3}$$

The absorption coefficient is the convolution of this population function with the homogeneous line shape:

$$\alpha(\nu) = \int N(\nu')\sigma\kappa(\nu' - \nu)d\nu' \tag{4}$$

and the transmitted intensity can be obtained from Beer's law. In order to determine the quantum efficiency, the total concentration of resonant ions and the transition oscillator strength must be known.

While it is not possible to find an analytical expression for the resulting burndown curve, numerical simulations were run with the hole burning quantum efficiency and homogeneous linewidth as parameters. The fitted and measured absorption coefficient and full width at half maximum (FWHM) of the hole are plotted as functions of time in Fig. 4, with the fit giving homogeneous linewidths of 13 and 16 MHz and quantum efficiencies of 8×10^{-4} and 2×10^{-3} for the L1 and L2 centers, respectively. It is clear that the increase of the hole width and the nonexponential hole growth are fundamental features of any simple model of spectral hole burning where the laser linewidth is narrower than the homogeneous linewidth.[28] The population of centers that

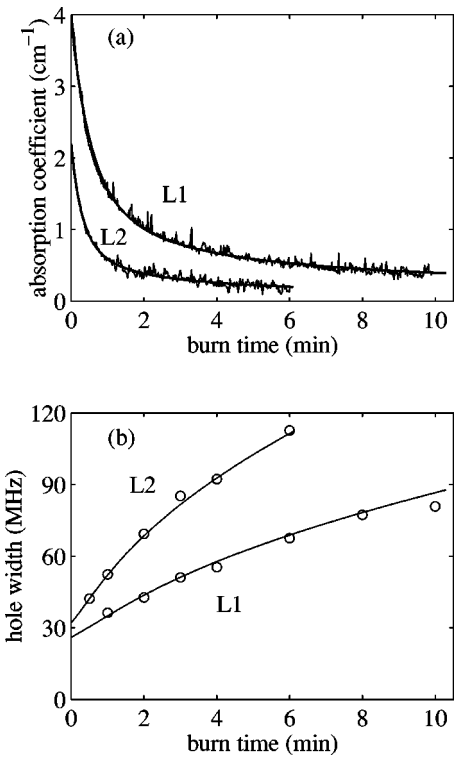

FIG. 4. Experimental and calculated burndown curves of (a) the hole depth and (b) the hole width of the L1 and L2 center spectral holes.

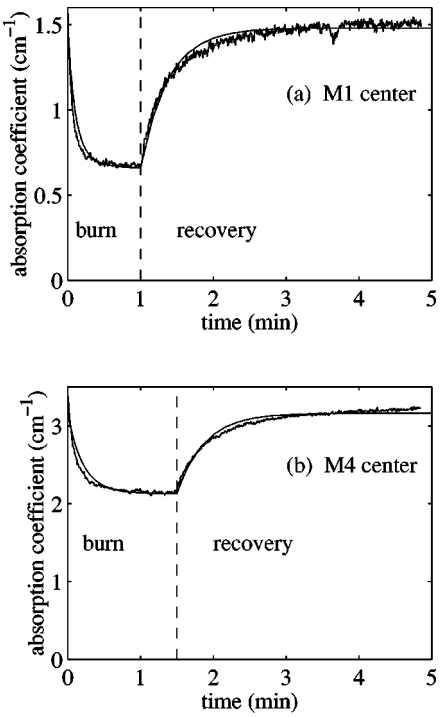

FIG. 5. Experimental and calculated burndown and recovery curves of the hole depth for (a) the M1 center and (b) the M4 center spectral holes.

have a small overlap of their homogeneous line with the laser frequency have a lower effective transition probability for absorption at the frequency of the laser and therefore bleach on a longer time scale than those having their homogeneous line centered at the laser frequency.

The close match of the experimental burndown curves with the functional form resulting from this simple model shows that it is not necessary to consider multiple quantum efficiencies arising from slightly inequivalent centers. Physically, this implies that the efficiency of the bleaching mechanism described in Sec. I B is not strongly affected by small perturbations of the crystal-field interaction.

For the M*i* family centers, an additional term needs to be added to represent power-independent refilling of the hole:

$$\frac{dN(\nu)}{dt} = -\frac{\eta I_0 N(\nu)\sigma\kappa(\nu_0-\nu)}{h\nu_0} + \frac{1}{\tau}[N_0(\nu)-N(\nu)], \tag{5}$$

where N_0 is the initial (equilibrium) value for the concentration of resonant ions and τ the hole recovery time constant. This will lead to exponential hole decay in the absence of laser irradiation, and a power-dependent saturation value (equilibrium level), as in the burndown curves for the M1 and M4 centers (Fig. 5). Fits to the model outlined above yield hole burning quantum efficiencies of 3×10^{-2} and 1×10^{-2} for the M1 and M4 centers, respectively. Figure 5 also shows the subsequent recovery of the hole peak, by continuing to measure the laser transmission with a 100-fold reduction in laser intensity. A filter originally placed in front of the photomultiplier tube was also removed at this time, so that the detected signal would be of a similar magnitude. Holes burned in the two lines have similar hole-recovery time constants of 23 s at a temperature of 1.7 K. This suggests that they may indeed belong to the same center, or at least have closely similar ion configurations.

Table II lists the hole burning quantum efficiencies and hole recovery time constants extracted from these fits, using the center concentrations estimated in Sec. II A. These quantum efficiencies are estimates only, with large uncertainty arising from the estimations of center concentrations and oscillator strengths. In particular, the apparent discrepancy between between the quantum efficiency values found for the M1 and M4 spectroscopic lines does not preclude the possibility that these lines are resonances associated with two crystal-field components of the excited state of the same spectroscopic Tm^{3+} center. However, it is evident that the M*i* centers have higher quantum efficiencies for hole burning than the L*i* centers. Together with the spontaneous hole recoverability of the M*i* centers, this indicates a much lower potential barrier for D^- ion displacement around the Tm^{3+} ion for the M*i* center configurations.

D. Temperature dependence

The temperature dependence of the hole burning process was investigated up to 30 K. Holes were burned and read at a series of temperatures from 2–30 K, with the laser fluence for hole burning fixed at 6 mW/cm^2 for 1 min. The widths (FWHM) of the resulting holes are plotted as a function of temperature in Fig. 6(a), and the hole depth is plotted against width in Fig. 6(b). As expected, holes burned at higher temperatures are broader, due to phonon-induced dephasing, and are therefore shallower. The solid curve in graph (b) represents hole depth and width calculated using the model of

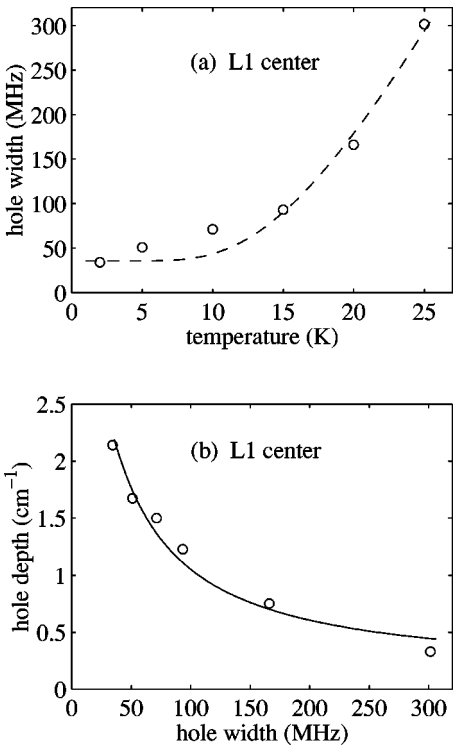

FIG. 6. Temperature dependence of L1-center spectral hole burning. Spectral holes were burned and read with the sample maintained at the stated temperatures. (a) hole width increase with temperature and (b) hole depth dependence on hole width. The solid line in (b) is from simulation, where the hole widths were taken as input parameters.

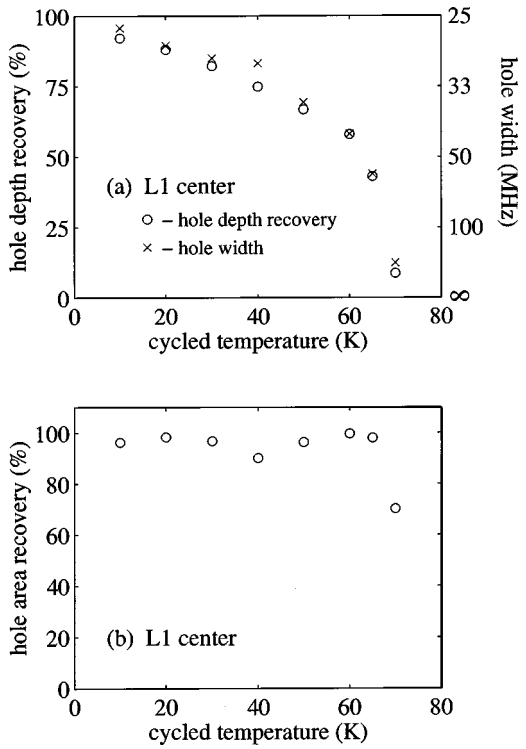

FIG. 7. Recovery of (a) the hole depth and (b) the inverse of the hole width of L1-center spectral holes, after cycling the sample to elevated temperatures. The similar functional forms show that the hole area is conserved for cycling up to at least 70 K.

Sec. II C, with the homogeneous linewidth the only varied parameter. The measured decrease in hole depth matches closely the expected behavior arising from homogeneous line broadening. The product of width and depth approximates the hole strength, and for fixed burn parameters this increases with temperature. This is not due to increased quantum efficiency, but rather is due simply to a higher rate of absorption for cases where the hole depth is shallower.

The homogeneous line broadening can be modeled as being caused by a single phonon annihilation process, where the phonon energy is resonant with a transition among crystal-field states within either the ground or excited manifold of the Tm^{3+} ion. The probability of such a phonon being absorbed is proportional to the phonon occupation number, and the temperature dependence of this mechanism for the homogeneous linewidth is

$$\Gamma(T)=\Gamma(0)+\frac{1}{\pi\tau}\exp\left(-\frac{\hbar\omega}{kT}\right). \tag{6}$$

The dashed line in Fig. 6(a) represents a fit to this model, giving a phonon energy of $40\pm10\ \mathrm{cm}^{-1}$. This does not match the known $96\ \mathrm{cm}^{-1}$ splitting in the $^3H_6$ ground state,[22] however the splitting of the $^3H_4$ excited state is not known and could account for the observed hole broadening.

E. Temperature cycling

An important hole burning parameter for device applications is the recoverability of the hole after cycling to elevated temperatures. In this experiment, holes were burned with the sample at 2 K, then the sample temperature was raised to the specified intermediate value and held there for 10 min, then recooled to 2 K before being remeasured. Some variation in the time at the elevated temperature arose as a consequence of the time taken to achieve the temperature ramp, which varied from 2–20 min depending on the temperature difference. The resulting changes in hole depth and width (on a reciprocal scale) are plotted in Fig. 7(a). There is some broadening of the holes, and with this broadening matching the decreasing hole depth, the area of the hole is conserved after cycling up to at least 70 K, as depicted in Fig. 7(b). For cycling to higher temperatures, the holes broaden to such an extent that they cannot be measured accurately for the burn parameters used. This broadening most likely arises from thermal relaxation of the D^- and CaF_2 lattice ion positions. These results show that thermally induced relocation of the D^- ions is inhibited up to at least 70 K, an important result for situations in which occasional sample heating may occur.

F. Estimate of barrier heights

We can place a lower limit on the barrier height W for the D^- ion relocalization of the L1 center by considering the thermal barrier hopping rate R to be given by the Arrhenius relation

$$R=\Omega_0\exp(-W/kT), \tag{7}$$

where Ω_0 is the attempt frequency. The fraction of centers that have not reverted to their original configuration after the hold time t_h is given by

$$f = \exp(-Rt_h). \quad (8)$$

These relations give a strong threshold for thermal barrier hopping at the temperature at which $f = 0.5$. If we take $\Omega_0 = 2 \times 10^{13}$ Hz as a typical attempt frequency corresponding to the ~ 700 cm^{-1} energy of the D^- vibrational modes, $t_h = 600$ s for the hold time at each elevated temperature, and the lower-limit threshold temperature of 70 K, we estimate a barrier height of $W = 1800$ cm^{-1}. This is in good agreement with values that have been determined for the analogous centers in $CaF_2:Pr^{3+}:D^-$ using broadband fluorescence bleaching.[29]

We can also estimate the barrier heights of the M1 and M4 centers. At a fixed temperature $1/R$ is the lifetime of the hole, measured to be 23 s at 1.7 K in Sec. II C. If we take the same value of Ω_0 as above, then we estimate a barrier height of $W = 40$ cm^{-1} for the M*i* centers, a factor of 50 smaller than for the L*i* centers. This is consistent with the M*i* centers having greater hole burning quantum efficiencies than the L*i* centers.

III. CONCLUSIONS

Spectral hole burning in the Tm^{3+} centers that are charge compensated by multiple D^- ions in $CaF_2:Tm^{3+}$ has been shown to yield long-term persistence for one family of centers. No measurable decay was observed over 48 h for the L1 center, with a similar result for the L2 center measured over 7 h. Transmission-peak and hole-width burndown curves for these centers were found to follow the behavior predicted by a simple model in which all resonant centers have the same hole burning quantum efficiency, and no reverse processes are allowed. Nonexponential decay, hole broadening with increasing burn time, and non-Lorentzian-shaped deep holes are all features that arise naturally within this model. The hole burning quantum efficiency in the L1 and L2 centers is $\sim 10^{-3}$. For applications requiring hole stability during long reading cycles, such as laser frequency references, this low efficiency is desirable. The L1 and L2 centers are robust under temperature cycling to at least 70 K, with the conserved hole areas demonstrating that reverse processes are not significant up to such temperatures. From this we estimate a lower limit on the D^- displacement barrier potential of 1800 cm^{-1}. Broadening of the holes with cycling is attributed to thermally induced relaxation of neighboring ion positions. Assuming that this is the important mechanism for hole relaxation, one may realistically expect very long persistence at low temperature.

A second family of centers, the M*i* centers, have hole burning quantum efficiencies approximately an order of magnitude higher than the L*i* centers, and spectral holes that decay with a time constant of approximately 23 s at 1.7 K giving an estimated D^- displacement barrier potential of 40 cm^{-1}. The hole-reversal processes responsible for this decay also give a power-dependent saturation level for the hole depth.

Hole widths measured for shallow holes varied from 18 to 40 MHz among the centers studied, and are possibly limited by instantaneous spectral diffusion effects from the D^- ion vibrations. The L1 center appears to be the prime candidate for hole burning applications as it has the highest absorption coefficient of the hole burning centers, has the narrowest holes, and has immeasurably small changes in hole width or area over a period of at least 48 h. In particular, we are exploring the application of laser frequency stabilization by reference to a spectral hole, and the L1 center of $CaF_2:Tm^{3+}:D^-$ is being used as a test bed for these reasons, and due to the availability of diode lasers at the 798 nm wavelength.

ACKNOWLEDGMENTS

Research at Montana State University was supported in part by U. S. Air Force Office of Scientific Research Grant Nos. F49620-96-1-0466 and F49620-98-0171. The crystal sample was grown and prepared under the guidance of Dr. Glynn D. Jones at the University of Canterbury, Christchurch, New Zealand.

[1] W. E. Moerner, in *Persistent Spectral Holeburning: Science and Applications*, edited by W. E. Moerner (Springer-Verlag, New York, 1988), Chap. 7.

[2] G. Castro, D. Haarer, R. M. Macfarlane, and H. P. Trommsdorff, U.S. Patent No. 4101976 (1978).

[3] A. R. Gutiérrez, J. Friedrich, D. Haarer, and H. Wolfrum, IBM J. Res. Dev. **26**, 198 (1982).

[4] T. W. Mossberg, Opt. Lett. **7**, 77 (1982).

[5] A. Rebane, R. Kaarli, P. Saari, A. Anijalg, and K. Timpmann, Opt. Commun. **47**, 173 (1983); A. K. Rebane, R. K. Kaarli, and P. M. Saari, Pis'ma Zh. Éksp. Teor. Fiz. **38**, 320 (1983) [JETP Lett. **38**, 383 (1983)]; A. Rebane and R. Kaarli, Chem. Phys. Lett. **101**, 317 (1983).

[6] X. A. Shen, E. Chiang, and R. Kachru, Opt. Lett. **19**, 1246 (1994); X. A. Shen, A.-D. Nguyen, J. W. Perry, D. L. Huestis, and R. Kachru, Science **278**, 96 (1997).

[7] G. C. Bjorklund, U.S. Patent No. 4306771 (1981).

[8] H. Sónajalg, A. Gorokhovskii, R. Kaarli, V. Palm, M. Rätsep, and P. Saari, Opt. Commun. **71**, 377 (1989).

[9] H. Schwoerer, D. Erni, A. Rebane, and U. P. Wild, Adv. Mater. **7**, 457 (1995).

[10] A. Renn, A. J. Meixner, U. P. Wild, and F. A. Burkhalter, Chem. Phys. **93**, 157 (1985); A. J. Meixner, A. Renn, and U. P. Wild, J. Chem. Phys. **91**, 6728 (1989); E. S. Maniloff, S. B. Altner, S. Bernet, F. R. Graf, A. Renn, and U. P. Wild, Appl. Opt. **34**, 4140 (1995); B. Plagemann, F. R. Graf, S. B. Altner, A. Renn, and U. P. Wild, Appl. Phys. B: Lasers Opt. **B66**, 67 (1998).

[11] G. C. Bjorklund and G. T. Sincerbox, U.S. Patent No. 4533211 (1985).

[12] P. Schätz, U. Bogner, and M. Maier, Appl. Phys. Lett. **49**, 1132 (1986); N. Hartmannsgruber, U. Bogner, and M. Maier, Opt. Quantum Electron. **23**, 361 (1991).

[13] U. P. Wild, A. Renn, C. De Caro, and S. Bernet, Appl. Opt. **29**, 4329 (1990).

[14] R. M. Macfarlane and R. M. Shelby, in *Spectroscopy of Rare-Earth Ions in Solids*, edited by A. A. Kaplyanskii and R. M.

Macfarlane (North Holland, Amsterdam, 1987), Chap. 3; in *Persistent Spectral Holeburning: Science and Applications*, (Springer-Verlag, New York, 1988), Chap. 4; Opt. Lett. **9**, 533 (1984); A. Winnacker, R. M. Shelby, and R. M. Macfarlane, *ibid.* **10**, 350 (1985).

[15] R. M. Macfarlane and G. Wittmann, Opt. Lett. **21**, 1289 (1996).

[16] D. M. Boye, R. M. Macfarlane, Y. Sun, and R. S. Meltzer, Phys. Rev. B **54**, 6263 (1996).

[17] R. M. Macfarlane, R. J. Reeves, and G. D. Jones, Opt. Lett. **12**, 660 (1987); R. J. Reeves and R. M. Macfarlane, J. Opt. Soc. Am. B **9**, 763 (1992).

[18] R. J. Reeves, G. D. Jones, and R. W. G. Syme, Phys. Rev. B **40**, 6475 (1989); R. J. Reeves, K. M. Murdoch, and G. D. Jones, J. Lumin. **66&67**, 136 (1995).

[19] K. Holliday and N. B. Manson, J. Phys.: Condens. Matter **1**, 1339 (1989).

[20] G. K. Liu and J. V. Beitz, Chem. Phys. Lett. **171**, 335 (1990).

[21] R. M. Macfarlane, Opt. Lett. **18**, 829 (1993).

[22] N. M. Strickland and G. D. Jones, Phys. Rev. B **56**, 10 916 (1997).

[23] N. J. Cockroft, G. D. Jones, and R. W. G. Syme, J. Chem. Phys. **92**, 2166 (1990).

[24] H. K. Welsh, J. Phys. C **18**, 5637 (1985).

[25] N. J. Cockroft, D. Thompson, G. D. Jones, and R. W. G. Syme, J. Chem. Phys. **86**, 521 (1987); T. P. J. Han, G. D. Jones, and R. W. G. Syme, Phys. Rev. B **47**, 14 706 (1993); G. D. Jones and K. M. Murdoch, J. Lumin. **60&61**, 131 (1994).

[26] D. R. Tallant, D. S. Moore, and J. C. Wright, J. Chem. Phys. **67**, 2897 (1977).

[27] W. E. Moerner, A. R. Chraplyvy, A. J. Sievers, and R. H. Silsbee, Phys. Rev. B **28**, 7244 (1983).

[28] S. Voelker, R. M. Macfarlane, A. Z. Genack, and H. P. Trommsdorff, J. Chem. Phys. **67**, 1759 (1977); K. K. Rebane and L. A. Rebane, in *Persistent Spectral Holeburning: Science and Applications*, edited by W. E. Moerner (Springer-Verlag, New York, 1988), Chap. 2.

[29] K. M. Murdoch and G. D. Jones, Phys. Rev. B **58**, 12 020 (1998).